Rapid Communications

Strongly extended diffusion length for the nonequilibrium magnons in $Y_3Fe_5O_{12}$ by photoexcitation

S. H. Wang,[1] G. Li,[2] E. J. Guo,[3] Y. Zhao,[1] J. Y. Wang,[1] L. K. Zou,[4] H. Yan,[1] J. W. Cai,[2] Z. T. Zhang,[1] M. Wang,[1] Y. Y. Tian,[1] X. L. Zheng,[2] J. R. Sun,[2,*] and K. X. Jin[1,†]

[1]*Shanxi Key Laboratory of Condensed Matter Structures and Properties, School of Science, Northwestern Polytechnical University, Xi'an 710072, China*

[2]*Beijing National Laboratory for Condensed Matter and Institute of Physics, Chinese Academy of Sciences, Beijing 100190, China*

[3]*Quantum Condensed Matter Division, Oak Ridge National Laboratory, Oak Ridge, Tennessee 37831, USA*

[4]*High Magnetic Field Laboratory, Chinese Academy of Science, 230031 Hefei, China*

(Received 17 December 2017; revised manuscript received 3 March 2018; published 9 May 2018)

$Y_3Fe_5O_{12}$ (YIG) is known for its long magnon diffusion length. Although it has the known lowest damping rate, an even longer diffusion distance is still highly desired since it may lead to a much more efficient information transmission and processing. While most of previous works focused on the generation and detection of magnons in YIG, here we demonstrate how to depress the damping rate during the diffusion of magnon. By selectively exciting the spin state transition of the Fe ions in YIG, we successfully increase magnon diffusion length by one order of magnitude, i.e., from the previous reported ∼10 μm up to ∼156 μm (for the sample prepared by liquid phase epitaxy) and ∼180 μm (for the sample prepared by pulsed laser deposition) at room temperature. The diffusion length, determined by nonlocal geometry, is ∼30 μm for the magnons induced by visible light and above 150 μm for the laser of 980 nm. In addition to thermal gradient, light excitation affects the electron configuration of the Fe^{3+} ion in YIG. Long-wavelength laser is more effective since it causes a transition of the Fe^{3+} ions in FeO_6 octahedron from a high spin to a low spin state and thus causes a magnon softening which favors a long-distance diffusion. The present work paves the way toward an efficient tuning of magnon transport which is crucially important for magnon spintronics.

DOI: 10.1103/PhysRevMaterials.2.051401

Magnons describe the deviation of a magnetic system from the fully magnetic order. The effective tuning of the transport process of nonequilibrium magnons may lead to a low energy-consumption technology for information storage, transmission, and processing. It therefore has attracted increasing attention in recent years. Nonequilibrium magnons can be generated by a thermal gradient across a magnet based on the spin Seebeck effect (SSE) which has been observed in a wide range of materials including ferrimagnetic [1–5], antiferromagnetic [6], and even some paramagnetic materials [7]. The diffusion of these magnons forms magnon current or spin current. By injecting the spin current into a heavy metal [1,8–10] or a topological insulator [11], which has a strong spin-orbit coupling and thus a strong inverse spin Hall effect (ISHE), the spin current will be converted into charge current which can be feasibly detected.

Magnon diffusion length is an important parameter characterizing the performance of the spintronic material. In fact, great efforts have been devoted to the determination of the magnon diffusion distance in $Y_3Fe_5O_{12}$ (YIG). A recent report showed that the SSE first increased and then saturated as the YIG film thickness increased [12,13]. At room temperature, the typical thickness for the saturation is ∼0.1 μm for the pulsed laser deposited (PLD) YIG film and ∼1 μm for the liquid-phase epitaxy (LPE) YIG film. Using laser illumination to locally break the thermal equilibrium between magnons and phonons, which can be directly probed by micro-Brillouin light scattering, An *et al.* [14] found that the magnon diffusion length in the bulk crystal YIG is about 3.1 μm at 372 K. Recently, nonlocal spin Seebeck geometry [15–20] was widely adopted to investigate spin transport behavior; the spatially separated structure makes the measurements immune to parasitic thermoelectric effect [21,22]. Through a spin accumulation in Pt in a nonlocal structure, the magnons can be generated and detected in a separated structure. Utilizing this structure, Cornelissen *et al.* [15] found that the magnon diffusion length is ∼9.4 μm at room temperature for the YIG film prepared by LPE. Focusing a laser spot on a Pt absorption pad to generate thermal magnons and detecting the ISHE signals from a Pt bar separated from the laser spot [16,18], Giles *et al.* observed two characteristic decay lengths for magnon spin currents in crystal bulk YIG: The rapid decay process is attributed to the gradient in the magnon chemical potential which is 20 μm and independent on temperature, and the slow decay process results from the gradient in magnon temperature which is 80 μm at 10 K.

There are dozens of articles which deal with the samples grown by different techniques, including LPE [15], PLD [12], and chemical solution method [23]. The samples quality could be different, resulting in the dispersion of the experimental data. For example, the reported magnon diffusion distance varies from 0.1 to 20 μm [12,18]. This calls for not only a further study on magnon diffusion in high-quality YIG but

*Author to whom correspondence should be addressed: jrsun@iphy.ac.cn

†Author to whom correspondence should be addressed: jinkx@nwpu.edu.cn

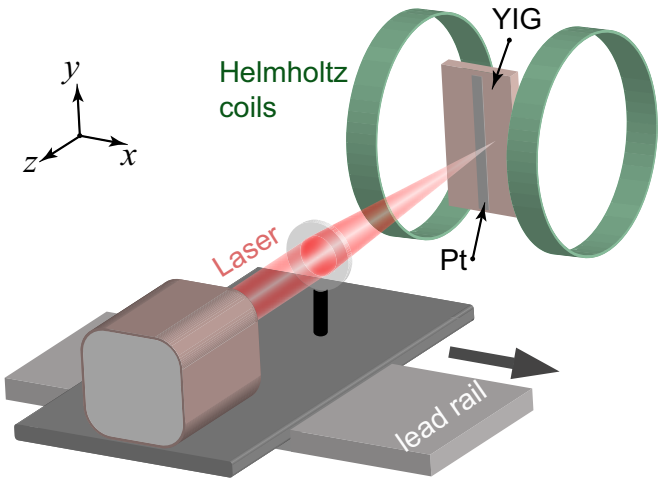

FIG. 1. A schematic diagram of the experimental setup.

also an exploration for key factors affecting magnon diffusion. As documented above, most of the previous works focused on the determination of the diffusion length. However, to find an effective approach that depresses the damping rate of the nonequilibrium magnon is more important and yet more challenging. Here we demonstrate how to extend the diffusion distance of the magnons in YIG. By selectively exciting the spin state of the Fe ions in YIG, we are successful in increasing the magnon diffusion length by one order of magnitude, i.e., from the original value of about 10 μm up to ~156 μm (for the LPE sample) and 180 μm (for the PLD sample) at room temperature. We also present evidence that the photoexcitation has caused a transition in electron configuration of the Fe^{3+} ions at special crystal sites of YIG, consistent with the earlier observation of variation of the Fe^{3+} ion electron configuration in light [24,25]. This in turn strongly modifies the dispersion relation of the magnon and thus the diffusion behavior of the magnon. Here we report the tuning of the transport process of thermal magnons, which opens an avenue for the manipulation of magnons in YIG.

YIG films were grown on (111)-oriented $Gd_3Ga_5O_{12}$ substrates ($5 \times 3 \times 0.5\,mm^3$) by the techniques of pulsed laser deposition and liquid phase epitaxy, respectively, with the corresponding film thicknesses of 40 nm and 20 μm. Then a Pt layer with a thickness of 5 nm was deposited by magnetron sputtering on the middle of YIG through a bar-shaped mask. The size of the Pt strip was $4.8 \times 0.5\,mm^2$. Further details on the sample characterizations and experimental setup can be found in the Supplemental Material [26].

Figure 1 is a sketch of the experiment setup. The laser and the convex mirror are mounted on a lead rail along the x axis, which allows a position tuning in micrometers. When the top surface of the sample is illuminated by a laser beam, the YIG film will absorb a part of the energy. In general, the absorbed energy will establish an out-of-plane thermal gradient, generating thermal magnons due to the SSE. The thermal magnons will then diffuse laterally toward the Pt bar, yielding an electrical voltage (V_{ISHE}) due to the ISHE. The ISHE voltage is calculated by $V_{ISHE} = [V_{ISHE}(+H) - V_{ISHE}(-H)]/2$, where $V_{ISHE}(+H)$ and $V_{ISHE}(-H)$ are the saturation voltages in two oppositely directed magnetic fields. Although an in-plane thermal gradient could also be produced by the absorbed energy, it will mainly locate at the region of the laser spot and decays rapidly in the lateral direction. As proven by the results of the finite-element model (FEM) simulation (see the Supplemental Material for FEM simulation in Fig. S3 [26]), the temperature of the YIG surface will return to ambient temperature within 15 μm [14,16]. Therefore, the lateral heat flow should have no detectable effect on the measurement of diffusion length.

Figure 2(a) shows the V_{ISHE} as a function of the absorbed laser power for the YIG film prepared by LPE. The absorbed power is the difference of the incident power from the reflected and transmitted power, measured by optical power meters. When the laser beam is focused on the middle of the Pt bar, V_{ISHE} linearly increases with laser power as expected. For clarity, the V_{ISHE} induced by the laser with the wavelength of λ nm is denoted as V^{λ}_{ISHE}. When covering the whole YIG with a Pt layer (5 nm in thickness), we observe that V_{ISHE} remains constant, regardless of the location and size of the laser spot (see Fig. S4 in the Supplemental Material for detailed measurements) [26]. V^{808}_{ISHE} and V^{980}_{ISHE} are larger than the V_{ISHE} induced by visible light. This is ascribed to the increased number of long-wavelength magnons induced by infrared light which will be discussed below.

Figure 2(b) presents the dependence of the normalized V_{ISHE} on the position of the laser spot. Setting the middle of the Pt electrode to $x = 0$, and collecting V_{ISHE} as the laser spot sweeps along the x axis, we found that the V_{ISHE} kept nearly constant when the laser spot scans across the Pt strip (-0.25 mm $< x < 0.25$ mm), and exponentially decreased with the distance away from the Pt bar. Fascinatingly, the decay rate strongly depends on wavelength. Illuminated by visible light (405, 532, and 605 nm), V_{ISHE} drops to zero immediately when the light spot moves out of the region of the Pt bar. In contrast, it decays slowly with the distance from Pt for the light of 808 and 980 nm, remaining sizable when the laser spot is 0.5 mm away from the Pt edge. A further analysis indicates that the V^{λ}_{ISHE}-x relation can be well described by [solid curves in Fig. 2(b)]

$$V^{\lambda}_{ISHE} = V^{\lambda}_{0} \exp\left(-\frac{x}{\xi^{\lambda}}\right), \tag{1}$$

where V^{λ}_{0} is the normalized coefficient and ξ^{λ} is the diffusion length of magnons induced by the laser of λ nm. The inset plot in Fig. 2(c) depicts the magnon diffusion distance as a function of laser wavelength. The thermal magnons generated by long-wavelength lasers transport much longer distances than that induced by short-wavelength lights. The diffusion lengths ξ^{405}, ξ^{532}, and ξ^{650} are all around 30 μm while ξ^{808} is ~137 μm and ξ^{980} is 156 μm, and the diffusion length is not sensitive to laser power as shown in [26] (see Supplemental Material for detailed measurements in Fig. S6 [26]). Increasing laser power causes a slight increase in ξ (see Fig. S6 in the Supplemental Material for detailed measurements [26]). The changes of ξ^{405} and ξ^{808} are only about 9 and 20 nm as the absorbed laser power increases, respectively. Therefore, the changes of ξ^{808} and ξ^{405} caused by thermal effect account for at most 15% of ($\xi^{808} - \xi^{405}$). This is a surprising result. It means that photoexcitation

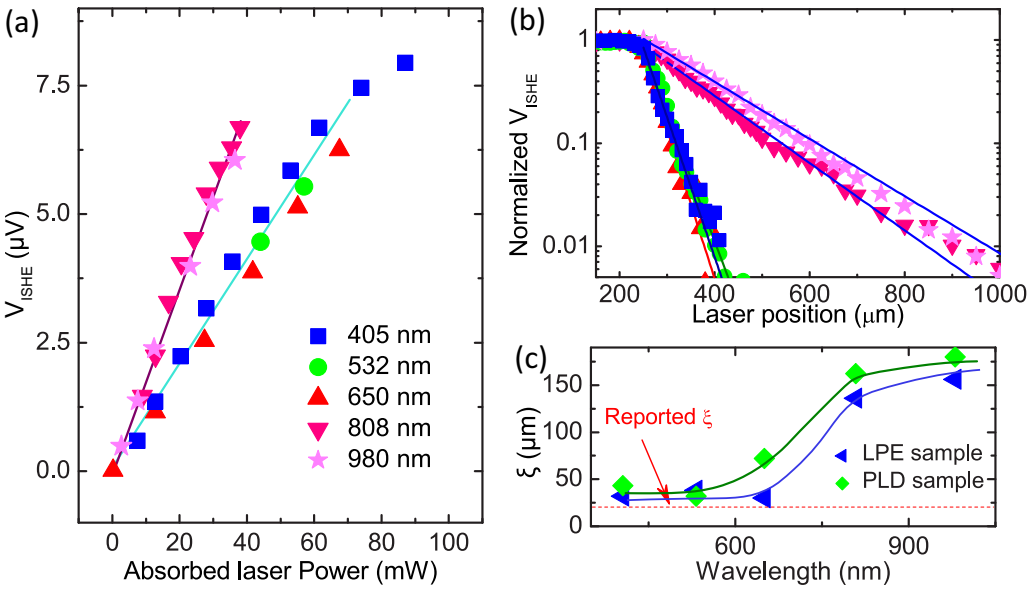

FIG. 2. (a) V_{ISHE} as a function of the absorbed laser power, measured with the lasers of different wavelengths. Laser spot was positioned at the middle of the Pt bar ($x = 0$). (b) Normalized V_{ISHE} as a function of spot position. The absorbed laser power is set to 30 mW. Symbols represent the experimental data and solid lines are the results of curve fitting based on Eq. (1). Only the data for the YIG prepared by LPE are shown here. (c) shows the diffusion length ξ as a function of laser wavelength, deduced from data fitting. Dashed red line is the previous reported longest diffusion length. All measurements were conducted at room temperature. The solid lines in (a) and (c) are guides to the eyes.

has increased the diffusion length of magnons in YIG by one order of magnitude at the ambient temperature, compared to the previous reported diffusion length [dashed line in Fig 2(c)] of 10–20 μm [15,18,19].

We also perform the same investigations for the thinner YIG film prepared by the PLD technique (40 nm), and observe similar phenomena (see Supplemental Material for detailed measurements in Fig. S5 [26]). It indicates that the strong tuning of magnon diffusion by photoexcitation is a general feature for the YIG. Meanwhile, it reveals that the film thickness independence of the magnon diffusion along the film plane is consistent with the previous report [17]. A careful inspection indicates that the diffusion length in PLD-prepared YIG is a slightly larger than that in LPE-prepared YIG. For example, ξ^{980} reaches a value as large as 180 μm. This is due to the fact that the sample prepared by PLD has a smoother surface (see Supplemental Material [26]) which will depress the magnon scattering during the lateral transportation. In the visible limit and the infrared light limit the two ξ-λ curves for the PLD-prepared YIG and LPE-prepared YIG coincide well with each other. This implies that the photoexcitation-enhanced magnon diffusion should be an intrinsic property of the YIG. We also noticed the difference of ξ at $\lambda =$ 650 nm for these two samples. Since 650 nm is a wavelength intermediating the dramatic transition from visible to infrared lights, its effect could be sensitive to sample quality. Obviously, the PLD-prepared YIG and the LPE-prepared YIG could not be exactly the same in quality.

To further verify that the long-range magnon diffusion length comes reliably from photoexcitation, we repeated the measurements after partially covering the sample by a reflected layer or an absorbed layer. This layer shields the YIG film from photoexcitation but the heating effect remains (see the Supplemental Material for an experiment for the argument of the longer magnon diffusion length induced by infrared light in Fig. S7 [26]). All the experimental results show that the diffusion length of the thermal magnon generated by photoexcitation is greater than that by the simple heating effect. Moreover, the infrared light is more effective in extending the diffusion distance than visible lights.

The amplification of magnon diffusion length is also observed at low temperatures. Figure 3 shows the temperature dependence of the diffusion length of magnons. According to the Bose-Einstein distribution, the amount of thermal magnons and phonons will decrease with decreasing temperature. This means that the scattering between magnons and phonons will be weakened, and the diffusion distance will be increased.

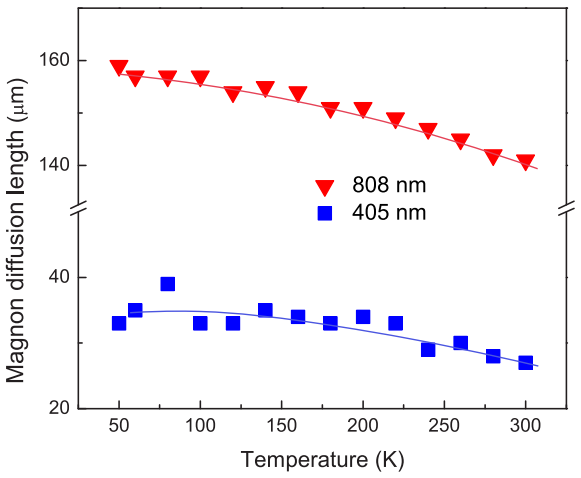

FIG. 3. Temperature dependence of thermal magnon diffusion length. The absorbed laser power is fixed at 30 mW. The solid lines are guides to the eyes.

Guo *et al.* [13] found that $\xi \propto T^{-1}$, i.e., diffusion length is closely related to the number of phonons and magnons. On the contrary, a previous study [20] with nonlocal geometry found a slight reduction of ξ with decreasing temperature, and ascribed this phenomenon to a compensation effect of increased relaxation time by reduced thermal velocity of the magnon. However, Fig. 3 shows that both ξ^{405} and ξ^{808} are only slightly increased upon cooling, rather than proportional to T^{-1} or slightly decreasing. The different ξ -T dependence in Fig. 3 implies that the diffusion behavior of the nonequilibrium magnon induced by light irradiation is unique.

Our observation cannot be ascribed to the so-called photo-spin-voltaic effect. A recent study showed that when the Pt/YIG hybrid structure is exposed to light, especially infrared light, a photon-driven spin-dependent electron excitation will occur near the Pt-YIG interface, producing a photo-spin-voltaic effect [27]. Since this effect is independent of the direction of temperature gradient, reversing the direction of thermal gradient will not change its sign. We reverse the incident direction of the light ($\lambda = 808$ nm) and find a sign change of V_{ISHE} (see the Supplemental Material for experiment for exclusion of the photo-spin-voltaic effect in Fig. S8 [26]). Moreover, illuminating the back side of the sample produces the same magnon diffusion length as illuminating the front side [26]. All these show that the V_{ISHE} detected here is unambiguously generated by nonequilibrium magnons instead of the photo-spin-voltaic effect.

The extended diffusion length and its strong-wavelength dependence observed here indicate that the light not only acts as a heating source to generate thermal gradient but also affects, in some way, the characteristics of the thermal magnon, assigning the latter unusual diffusion properties. To see what has happened to the YIG under laser illumination, we measured the absorption spectrum of YIG. As shown in Fig. 4, there are four broad absorption peaks locating at ~400, ~530, ~650, and ~900 nm, respectively. According to earlier research [24,25], the peak around 800–1000 nm arises from the ${}^6A_{1g}({}^6S) \rightarrow {}^4T_{1g}({}^4G)$ transition of the electron configuration in

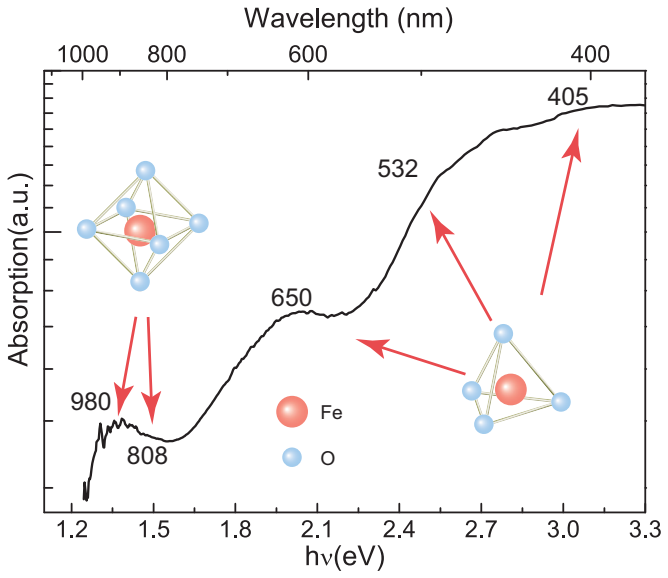

FIG. 4. Absorption spectrum of the YIG film prepared by PLD.

octahedral crystal field, while the 650, 530, and 400 nm peaks correspond to the ${}^6A_1({}^6S) \rightarrow {}^4T_1({}^4G)$, ${}^6A_1({}^6S) \rightarrow {}^4T_2({}^4G)$, and ${}^6A_1({}^6S) \rightarrow {}^4T_2({}^4D)$ transitions in the tetrahedral crystal field, respectively. Visible light may also be absorbed by the electron in octahedral crystal field. However, due to the octahedral symmetry, transitions between the ground state and any excited states are parity forbidden. As a result, the visible light is nearly totally absorbed by the electron in tetrahedral crystal field.

It is possible that the different effects of the visible and infrared lights stem from their different influences on the electron configurations of the Fe^{3+} ions in different crystal sites. As will be shown below, the variation in electron configurations will affect the dispersion relation of the magnon, thus magnon diffusion. As well established, two of the five Fe^{3+} ions in YIG are octahedrally coordinated (a sites) while the other three are tetrahedrally coordinated (d sites), forming two sublattices. The magnetic moments of the two sublattices arrange antiparallel to each other, i.e., the YIG is ferrimagnetic. The magnetic moment of the a-site (d-site) Fe^{3+} is antiparallel (parallel) to external magnetic field as well as the net magnetization. Denoting the superexchange interaction between the a-site and d-site Fe ions as J_{ad}, we have the dispersion relation for the acoustic branch spin wave [28]

$$\hbar\omega_q = 4a^2 \left| J_{ad} \frac{S_d S_a}{S_d - S_a} \right| q^2, \tag{2}$$

under long-wavelength approximation, where a, ω_q, and q are respectively lattice constant, the frequency, and wave vector of the magnon, and S_a and S_d are the spin quantum numbers of the Fe^{3+} ions at the a and d sites, respectively. In the derivation of Eq. (2), we have ignored the influence of J_{aa} and J_{dd} since they are much smaller than J_{ad} [29].

Obviously, the relaxation process will cause a dissipation of the magnons. The relaxation time τ has been calculated in many works [30,31]. Following the procedure in Ref. [31], it can be proven $\tau \sim D^{-1}$, where $D = 4a^2 |J_{ad} \frac{S_d S_a}{S_d - S_a}|$ is the stiffness constant of the magnon. There is a simple relation between diffusion length and the stiffness constant $\xi \sim D^{-0.5}$, adopting the relation $\xi \propto \tau^{0.5}$. Therefore, if the variation of D with the electron configuration transition is known, the diffusion behavior of the magnons would be understood.

A simple analysis shows that a direct consequence of the ${}^6A_{1g} \rightarrow {}^4T_{1g}$, ${}^6A_1 \rightarrow {}^4T_1$, and ${}^6A_1 \rightarrow {}^4T_2$ switching is spin state transition; the number in the upper left corner of each symbol is $2S + 1$, with S being the spin angular quantum number of Fe^{3+}. The ground state and the excited state are a high-spin state and a low-spin state, respectively. When the spin state of the Fe^{3+} ion at a site (d site) changes from high spin state to low spin state under illumination, it will cause a reduction of $S_a(S_d)$. Corresponding to the high spin state ($S_d = 3 \times 5/2$) to low spin state ($S_d = 3 \times 3/2$) transition of the d-site Fe^{3+} ion (three of the five Fe^{3+} ions are tetrahedrally coordinated), a direct calculation gives variation of $\frac{S_d S_a}{S_d - S_a}$ from 15 to 45. In contrast, when the a-site Fe^{3+} ion changes from high spin state ($S_a = 2 \times 5/2$) to low spin state ($S_a = 2 \times 3/2$) (two of the five Fe^{3+} ions are octahedrally coordinated), $\frac{S_d S_a}{S_d - S_a}$ will increase from 15 to 5. From visible to infrared light, the $\frac{S_d S_a}{S_d - S_a}$ term is reduced by a factor of 9. In addition to $\frac{S_d S_a}{S_d - S_a}$, J_{ad} is also a factor affecting the dispersion relation. According to

the theory of superexchange [32], J_{ad} is proportional to Δ^{-2}, where $\Delta = E_d - E_p$, is the energy difference between the $3d$ and $2p$ orbital states of the magnetic ion and the oxygen ion, respectively. The energy splitting of the $3d^5$ state is strongly dependent on the configuration of the surrounding oxygen ions. E_d will grow when the electron transfers from the ${}^6A_{1g}({}^6S)$ to the ${}^4T_{1g}({}^4G)$ configuration, causing a decrease in J_{ad}. For the tetrahedral crystal field, according to Eq. (2) the effects of the spin state transition and the variation of J_{ad} counteract each other. For the octahedral crystal field, on the contrary, the two effects enhance each other, making the magnons softened.

Therefore, Fig. 4 presented evidence for the ${}^6A_{1g}\rightarrow{}^4T_{1g}$, ${}^6A_1\rightarrow{}^4T_1$, and ${}^6A_1\rightarrow{}^4T_2$ transitions. These transitions are actually spin state transitions which have been clearly addressed by earlier reports [24]. Meanwhile, J_{ad} will decrease due to the growth of occupied $3d$ orbital states of the magnetic ion induced both by infrared and visible light. And these will affect the stiffness of the magnon and thus the diffusion distance due to $\xi \sim D^{-1/2}$.

It is worth mentioning that the lateral magnon diffusion length deduced from the nonlocal geometry could be substantially different from the diffusion length derived from the local configuration. In the latter case the spin current is parallel to temperature gradient, thus it suffers from the scattering of surface and interface [12,13]. Meanwhile, as proven by recent investigations, the SSE mainly originated from long-wavelength magnons [33,34]. Therefore, the magnons detected here are mainly long-wavelength ones which present a lower relaxation rate [35]. This is one of the reasons why the diffusion distance here is longer than that determined by other techniques such as Brillouin scattering which takes the thermal magnons of the whole spectrum into account [14]. If only the magnons below a threshold wave vector q_{eff} contribute to the SSE, their number will be

$$n_{\mathrm{eff}} = \int_0^{q_{\mathrm{eff}}} g(\omega_q) n_q dq, \tag{3}$$

where $g(\omega_q)$ is the density of mode which is

$$g(\omega_q) = \frac{Vq^2}{\pi^2}\frac{dq}{d\omega} \tag{4}$$

for the three-dimensional system where V is the volume of the sample, and n_q is the Bose-Einstein distribution for magnons. So, we get

$$n_{\mathrm{eff}} = \int_0^{q_{\mathrm{eff}}} \frac{Vq}{2D\pi^2}\frac{1}{\exp[\hbar Dq^2/k_{\mathrm{B}}T]-1}dq. \tag{5}$$

It is obvious that decreasing the spin stiffness D will increase the number of the effective magnons which contributes to the SSE. This is the reason why the infrared light can induce larger V_{ISHE} than the visible light with the same absorbed power as shown in Fig. 2(a).

We also noticed the works by Giles *et al.* [18] on the two exponential decays. The shorter one is attributed to the gradient in the magnon chemical potential (λ_1), and the longer one results from the gradient in magnon temperature (λ_2). We observed essentially only one decay process both in room and low temperature. Possibly, the reported decay length of the first process is shorter than 10 μm, which is close to the size of our laser spot, and cannot be identified from the present data. Meanwhile, they use a Pt pad to absorb the light energy and generate thermal gradient, and reported a diffusion length of 20 μm at 250 K [16,18]. As demonstrated by our experiments [26], the diffusion length is very short for magnons induced by thermal gradient alone, which is a conclusion consistent with that of Giles *et al.* Of course, the incident light in the work of Giles *et al.* may also be transmitted to YIG through the Pt pad. However, the Pt pad is 10 nm in thickness, and the transmitted intensity could be too weak to produce any significant effects on the electron configuration.

In summary, we experimentally show that the diffusion length of the nonequilibrium magnons in YIG is strongly dependent on laser wavelength when they are induced by laser irradiation. Magnons generated by the laser beams of 808 and 980 nm can be detected from a distance as far as 1 mm. The corresponding diffusion lengths are 137 and 156 μm, respectively, while the diffusion length of the magnons excited by visible light (400–650 nm) is only ~30 μm. We found unambiguous correspondences between the electron configuration and magnon diffusion. A long-wavelength laser excites a transition of the electron configuration for the FeO_6 octahedron in YIG and induces softened magnons which have a longer diffusion distance. In contrast, visible light only affects electron configuration in the FeO_4 tetrahedron, and the corresponding magnons are relatively stiff. The present work demonstrates the tuning of magnon diffusion by selective modification of electron configuration. The principle proven here can be extended to other materials.

This work is supported by the National Natural Science Foundation of China (Grants No. 11604265, No. 51402240, No. 11520101002, and No. 51572222) and the Fundamental Research Funds for the Central Universities (Grant No. 3102017jc01001). J.R.S. acknowledges the support of the National Basic Research of China (Grant No. 2016YFA0300701) and Key Program of the Chinese Academy of Sciences.

[1] K. Uchida, H. Adachi, T. Ota, H. Nakayama, S. Maekawa, and E. Saitoh, Observation of longitudinal spin-Seebeck effect in magnetic insulators, Appl. Phys. Lett. **97**, 172505 (2010).

[2] R. Ramos, T. Kikkawa, K. Uchida, H. Adachi, I. Lucas, M. H. Aguirre, P. Algarabel, L. Morellón, S. Maekawa, E. Saitoh *et al.*, Observation of the spin Seebeck effect in epitaxial Fe_3O_4 thin films, Appl. Phys. Lett. **102**, 072413 (2013).

[3] J. Barker and G. E. W. Bauer, Thermal Spin Dynamics of Yttrium Iron Garnet, Phys. Rev. Lett. **117**, 217201 (2016).

[4] J. Cramer *et al.*, Magnon mode selective spin transport in compensated ferrimagnets, Nano Lett. **17**, 3334 (2017).

[5] S. Wang, L. Zou, X. Zhang, J. Cai, S. Wang, B. Shen, and J. Sun, Spin Seebeck effect and spin Hall magnetoresistance at

high temperatures for a Pt/yttrium iron garnet hybrid structure, Nanoscale **7**, 17812 (2015).

[6] S. Seki, T. Ideue, M. Kubota, Y. Kozuka, R. Takagi, M. Nakamura, Y. Kaneko, M. Kawasaki, and Y. Tokura, Thermal Generation of Spin Current in an Antiferromagnet, Phys. Rev. Lett. **115**, 266601 (2015).

[7] S. M. Wu, J. E. Pearson, and A. Bhattacharya, Paramagnetic Spin Seebeck Effect, Phys. Rev. Lett. **114**, 186602 (2015).

[8] K. Uchida, M. Ishida, T. Kikkawa, A. Kirihara, T. Murakami, and E. Saitoh, Longitudinal spin Seebeck effect: from fundamentals to applications, J. Phys.: Condens. Matter **26**, 343202 (2014).

[9] D. Magginetti, K. Tian, and A. Tiwari, β-Tantalum, a better candidate for spin-to-charge conversion, Solid State Commun. **249**, 34 (2017).

[10] L. Liu, C.-F. Pai, Y. Li, H. W. Tseng, D. C. Ralph, and R. A. Buhrman, Spin-torque switching with the giant spin Hall effect of tantalum, Science **336**, 555 (2012).

[11] Z. Jiang, C.-Z. Chang, M. R. Masir, C. Tang, Y. Xu, J. S. Moodera, A. H. MacDonald, and J. Shi, Enhanced spin Seebeck effect signal due to spin-momentum locked topological surface states, Nat. Commun. **7**, 11458 (2016).

[12] A. Kehlberger, U. Ritzmann, D. Hinzke, E.-J. Guo, J. Cramer, G. Jakob, M. C. Onbasli, D. H. Kim, C. A. Ross, M. B. Jungfleisch, B. Hillebrands, U. Nowak, and M. Kläui, Length Scale of the Spin Seebeck Effect, Phys. Rev. Lett. **115**, 096602 (2015).

[13] E.-J. Guo, J. Cramer, A. Kehlberger, C. A. Ferguson, D. A. MacLaren, G. Jakob, and M. Kläui, Influence of Thickness and Interface on the Low-Temperature Enhancement of the Spin Seebeck Effect in YIG Films, Phys. Rev. X **6**, 031012 (2016).

[14] K. An, K. S. Olsson, A. Weathers, S. Sullivan, X. Chen, X. Li, L. G. Marshall, X. Ma, N. Klimovich, J. Zhou, L. Shi, and X. Li, Magnons and Phonons Optically Driven out of Local Equilibrium in a Magnetic Insulator, Phys. Rev. Lett. **117**, 107202 (2016).

[15] L. J. Cornelissen, J. Liu, R. A. Duine, J. B. Youssef, and B. J. van Wees, Long-distance transport of magnon spin information in a magnetic insulator at room temperature, Nat. Phys. **11**, 1022 (2015).

[16] B. L. Giles, Z. Yang, J. S. Jamison, and R. C. Myers, Long-range pure magnon spin diffusion observed in a nonlocal spin-Seebeck geometry, Phys. Rev. B **92**, 224415 (2015).

[17] J. Liu, L. J. Cornelissen, J. Shan, T. Kuschel, and B. J. van Wees, Magnon planar Hall effect and anisotropic magnetoresistance in a magnetic insulator, Phys. Rev. B **95**, 140402 (2017).

[18] B. L. Giles, Z. Yang, J. S. Jamison, J. M. Gomez-Perez, S. Vélez, L. E. Hueso, F. Casanova, and R. C. Myers, Thermally driven long-range magnon spin currents in yttrium iron garnet due to intrinsic spin Seebeck effect, Phys. Rev. B **96**, 180412 (2017).

[19] J. Shan, L. J. Cornelissen, J. Liu, J. B. Youssef, L. Liang, and B. J. van Wees, Criteria for accurate determination of the magnon relaxation length from the nonlocal spin Seebeck effect, Phys. Rev. B **96**, 184427 (2017).

[20] L. J. Cornelissen, J. Shan, and B. J. van Wees, Temperature dependence of the magnon spin diffusion length and magnon spin conductivity in the magnetic insulator yttrium iron garnet, Phys. Rev. B **94**, 180402 (2016).

[21] S. Y. Huang, X. Fan, D. Qu, Y. P. Chen, W. G. Wang, J. Wu, T. Y. Chen, J. Q. Xiao, and C. L. Chien, Transport Magnetic Proximity Effects in Platinum, Phys. Rev. Lett. **109**, 107204 (2012).

[22] Y. M. Lu, Y. Choi, C. M. Ortega, X. M. Cheng, J. W. Cai, S. Y. Huang, L. Sun, and C. L. Chien, Pt Magnetic Polarization on $Y_3Fe_5O_{12}$ and Magnetotransport Characteristics, Phys. Rev. Lett. **110**, 147207 (2013).

[23] I. Lucas, P. Jiménez-Cavero, J. M. Vila-Fungueiriño, C. Magén, S. Sangiao, J. M. de Teresa, L. Morellón, and F. Rivadulla, Chemical solution synthesis and ferromagnetic resonance of epitaxial thin films of yttrium iron garnet, Phys. Rev. Mater. **1**, 074407 (2017).

[24] G. B. Scott, D. E. Lacklison, and J. L. Page, Absorption spectra of $Y_3Fe_5O_{12}$ (YIG) and $Y_3Ga_5O_{12}$: Fe^{3+}, Phys. Rev. B **10**, 971 (1974).

[25] S. H. Wemple, S. L. Blank, J. A. Seman, and W. A. Biolsi, Optical properties of epitaxial iron garnet thin films, Phys. Rev. B **9**, 2134 (1974).

[26] See Supplemental Material at http://link.aps.org/supplemental/10.1103/PhysRevMaterials.2.051401 for detailed sample characterization and experimental setup, magnon diffusion length of the film prepared by PLD, exclusion of photo-spin-voltaic effect, and so on.

[27] D. Ellsworth *et al.*, Photo-spin-voltaic effect, Nat. Phys. **12**, 861 (2016).

[28] J. Van Kranendonk and J. H. Van Vleck, Spin waves, Rev. Mod. Phys. **30**, 1 (1958).

[29] E. E. Anderson, Molecular field model and the magnetization of YIG, Phys. Rev. **134**, A1581 (1964).

[30] L. M. Woods, Magnon-phonon effects in ferromagnetic manganites, Phys. Rev. B **65**, 014409 (2001).

[31] M. Sparks, R. Loudon, and C. Kittel, Ferromagnetic relaxation. I. Theory of the relaxation of the uniform precession and the degenerate spectrum in insulators at low temperatures, Phys. Rev. **122**, 791 (1961).

[32] P. W. Anderson, Antiferromagnetism. Theory of superexchange interaction, Phys. Rev. **79**, 350 (1950).

[33] H. Jin, S. R. Boona, Z. Yang, R. C. Myers, and J. P. Heremans, Effect of the magnon dispersion on the longitudinal spin Seebeck effect in yttrium iron garnets, Phys. Rev. B **92**, 054436 (2015).

[34] T. Kikkawa, K.-i. Uchida, S. Daimon, Z. Qiu, Y. Shiomi, and E. Saitoh, Critical suppression of spin Seebeck effect by magnetic fields, Phys. Rev. B **92**, 064413 (2015).

[35] S. M. Rezende, R. L. Rodríguez-Suárez, R. O. Cunha, A. R. Rodrigues, F. L. A. Machado, G. A. F. Guerra, J. C. L. Ortiz, and A. Azevedo, Magnon spin-current theory for the longitudinal spin-Seebeck effect, Phys. Rev. B **89**, 014416 (2014).